# Antiproton Powered Propulsion with Magnetically Confined Plasma Engines

Michael R. LaPointe*
*Sverdrup Technology, Inc., Brook Park, Ohio 44142*

**Matter-antimatter annihilation releases more energy per unit mass than any other method of energy production, making it an attractive energy source for spacecraft propulsion. The use of highly energetic charged byproducts arising from proton-antiproton annihilation has been proposed for a variety of advanced propulsion schemes. Of these, the magnetically confined plasma engine may offer the most versatility in mission performance. Antiprotons are injected axially into a pulsed magnetic mirror system where they annihilate with an initially neutral hydrogen gas. The resulting charged annihilation byproducts are confined by the magnetic mirror system, which heat and ionize the hydrogen propellant. The magnetically confined ionized hydrogen plasma undergoes subsequent heating by the annihilation byproducts until expelled through one end of the magnetic mirror system, providing thrust. While allowing a wide range of specific impulse and thrust, the engine suffers from extremely low energy transfer efficiencies (≤ 1%). In addition, significant mass will be required to shield the superconducting magnet coils from high energy γ-radiation produced by neutral pion decay. The mass of the radiation shield may dominate the total engine mass, and will severely limit the performance of any antiproton powered engine which utilizes magnetic confinement. The problem is compounded in the antiproton powered plasma engine, where lower energy plasma bremsstrahlung radiation may cause shield surface ablation and degradation.**

## Nomenclature

| | | |
|---|---|---|
| $e^-$, $e^+$ | = | electron, positron |
| $I_{sp}$ | = | specific impulse (s) |
| MeV | = | $10^6$ electron volts ($1.602 \times 10^{-13}$ J) |
| $\dot{m}$ | = | mass flow rate (kg/s) |
| $n_\alpha$ | = | number density, species $\alpha$ |
| $Pn$ | = | protonium |
| $Ps$ | = | positronium |
| $p$, $\bar{p}$ | = | proton, antiproton |
| $Q_{e,i}$ | = | electron-ion energy exchange rate |
| $R_m$ | = | magnetic mirror ratio |
| $Th$ | = | thrust (N) |
| $V_c$ | = | chamber volume ($m^3$) |
| $v_{ex}$ | = | exhaust velocity (m/s) |
| $\alpha$ | = | ionization fraction |
| $\beta$ | = | velocity/speed of light |
| $\eta_i$ | = | energy transfer efficiency |
| $\lambda$ | = | rate coefficient ($s^{-1}$) |
| $\mu^+$, $\mu^-$ | = | charged muon, antimuon |
| $\nu_\mu$, $\bar{\nu}_\mu$ | = | mu-neutrino, anti-mu-neutrino |
| $\nu_e$, $\bar{\nu}_e$ | = | e-neutrino, anti-e-neutrino |
| $\pi^+$, $\pi^-$ | = | charged pion, antipion |
| $\omega_{pe}$ | = | electron plasma frequency ($s^{-1}$) |

## Introduction

OVER the past few decades, the combustion of chemical fuels has provided a satisfactory method of spacecraft propulsion. However, the limited energy available in chemical combustion is inadequate for several missions of interest, and the continued advancement of space exploration requires a commitment to develop new propulsion concepts. One of the more exotic reactions considered for advanced spacecraft propulsion is the annihilation of matter and antimatter. The energy released per kilogram of combined matter and antimatter is over 250 times the specific energy released in nuclear fusion, and over 8 orders of magnitude greater than the specific energy released in chemical combustion.[1] Efficiently transferring this reaction energy to a propellant could provide high thrust and optimum exhaust velocities without the inherent limitations imposed by chemical combustion energy or the mass penalties of external power supplies.

### Electron-Positron Annihilation

Direct annihilation of an electron ($e^-$) with a positron ($e^+$) proceeds via the reaction

$$e^- + e^+ \rightarrow 2\gamma \tag{1}$$

where each of the emitted γ-ray photons has an energy equal to half the sum of the rest mass plus kinetic energies of the electron-positron pair ($E_\gamma \geq 0.511$ MeV). An electron and positron may also undergo radiative capture to form a bound state of positronium ($Ps$) through the process

$$e^- + e^+ \rightarrow Ps + h\nu \tag{2}$$

Energetic γ-rays are then released upon the subsequent annihilation of the positronium.

The use of electron-positron annihilation energy to provide direct thrust or to heat an expellant for spacecraft propulsion was considered as early as 1953.[2] However, engine efficiency using a directed γ-ray exhaust is limited by the inability to effectively collimate the energetic photons. In addition, the γ-ray energy will not couple directly to a propellant, although it could be absorbed in a refractory metal heat exchanger and subsequently transferred to a flowing propellant. Of more fundamental concern, the storage density of positronium fuel may be so low that the mass of the positronium storage facility may overwhelm any potential benefit derived from electron-positron annihilation.[3]

Presented as Paper 89-2334 at the AIAA/ASME/ASCE/SAE 25th Joint Propulsion Conference, Monterey, CA, July 10–12, 1989. Received January 18, 1990; revision received Oct. 22, 1990; accepted for publication Oct. 24, 1990. 

*Advanced Propulsion Engineer, NASA Lewis Research Center Group, 2001 Aerospace Parkway. Member AIAA.

**Proton-Antiproton Annihilation**

Antiproton annihilation enjoys several advantages over positron annihilation as an energy source for spacecraft propulsion. The higher rest mass energies of the proton-antiproton ($p\bar{p}$) pair yield 1877 MeV per annihilation event, compared with the 1.02 MeV released by electron-positron annihilation. As discussed below, a significant fraction of the proton-antiproton annihilation energy appears in the kinetic energy of charged particles, which may be collimated for direct thrust or used to heat a propellant more effectively than the $\gamma$-radiation released in electron-positron annihilation.

Antiprotons and positrons may be cooled and combined to form antihydrogen.[4] Although it remains a technical challenge, it may be possible to further cool and condense the antihydrogen to form antihydrogen crystals.[3,4] Several schemes have been proposed to confine the antihydrogen "ice" using magnetic, electrostatic, or electromagnetic traps,[4,5] that yield a high storage density for the antiproton fuel. Electromagnetic radiation may be used to detach antihydrogen molecules or atoms from the surface of the crystal and ionize the antihydrogen into positrons and antiprotons.[5] The antiprotons may be guided with electric and magnetic fields to a reaction chamber, where they annihilate with protons to provide propulsive energy. The positrons, stripped from the antihydrogen atoms, could be used to provide auxiliary power for spacecraft components.[5]

Protons and antiprotons may undergo direct annihilation, or at low energies may form bound states of protonium ($Pn$) leading to subsequent annihilation.[6] Protonium may be formed as a result of radiative capture

$$p + \bar{p} \rightarrow Pn + h\nu \tag{3}$$

or by rearrangement collisions in a hydrogen gas

$$H + \bar{p} \rightarrow Pn + e^- \tag{4}$$

At low energies, $p\bar{p}$ annihilation proceeds via rearrangement collisions, while direct annihilation dominates at energies above roughly 10 eV. Radiative capture cross sections are not significant at energies above a fraction of an eV.

The general proton-antiproton annihilation scheme is outlined in Table 1. Each of the three charged pions has a rest mass energy of 139.6 MeV, and each of the two neutral pions has a rest mass energy of 135.0 MeV; thus a total of 689 MeV is contained in pion rest mass energies. The average kinetic energy of the charged pions is 250 MeV/pion,[7] thus 750 MeV or roughly 40% of the $p\bar{p}$ annihilation energy resides in charged pion kinetic energy. At this energy the charged pion is traveling with a velocity 93% the speed of light, and relativistic effects extend its lifetime from 26 ns at rest to approximately 70 ns. Unless acted upon, the charged pion will travel almost 21 meters before it decays. The remainder of the annihilation energy resides in the kinetic energy of the neutral pions, roughly 220 MeV/pion. At this energy the neutral pion lifetime is extended to $2.2 \times 10^{-16}$ seconds, and upon decay each neutral pion produces two energetic $\gamma$-rays, each with energies between 130 and 300 MeV/$\gamma$.

The decay of the $\pi^+$ or $\pi^-$ meson liberates an amount of energy equal to their rest mass energy and kinetic energy combined, or roughly 390 MeV/pion. The $\pi^+$ decays into a charged muon ($\mu^+$) and a mu-neutrino ($\nu_\mu$). The $\mu^+$ has a rest mass energy of 105.7 MeV and an average kinetic energy of 192.3 MeV/muon,[7] leaving the neutrino with roughly 90 MeV. The energetics are the same for the decay of the $\pi^-$ into a $\mu^-$ and an anti-$\mu$-neutrino ($\bar{\nu}_\mu$). The total kinetic energy of the three charged muons created by the decay of the three charged pions is thus 577 MeV, or about 31% of the initial $p\bar{p}$ annihilation energy. A charged muon with a kinetic energy of 192.3 MeV is traveling at 94% the speed of light, and its lifetime is extended from 2.2 to 6.2 $\mu$s. Unless acted upon, the muon will travel nearly 1800 meters before it decays. The neutrinos, traveling at the speed of light, will carry their energy out of the system.

The $\mu^+$ decays into a positron, an $e$-neutrino ($\nu_e$), and an anti-$\mu$-neutrino ($\bar{\nu}_\mu$), while the $\mu^-$ decays into an electron, a $\mu$-neutrino, and an anti-$e$-neutrino ($\bar{\nu}_e$). The total energy available from the charged muon decay is about 300 MeV/muon. Of this energy, 0.511 MeV goes into creating the electron or positron, about 100 MeV into the electron or positron kinetic energy,[7] and the remainder to the noninteracting neutrinos. Thus, the decay of the three charged muons arising in the $p\bar{p}$ annihilation scenario will provide roughly 300 MeV in the form of kinetic energy of the three electrons/positrons, corresponding to 16% of the initial proton-antiproton annihilation energy. The electrons and positrons are stable against decay, but can annihilate with one another to produce 0.511 MeV $\gamma$-rays, the ultimate end of the $p\bar{p}$ annihilation process.

**Antiproton Engine Concepts**

Several antiproton powered rocket designs have been suggested, ranging from the low thrust, high specific impulse pion engine to the high thrust, low specific impulse solid and gas core thermal rockets.[4] The former concept is restricted to interstellar or deep space missions which require relativistic exhaust velocities, while the latter concepts are limited in performance by thermal constraints on material walls. A design which appears to minimize material constraints while providing a range of operating parameters is the antiproton powered plasma rocket, which utilizes magnetic mirror fields to contain both the charged annihilation products and the ionized propellant.

Morgan[5] has sketched a preliminary design for a pulsed heavy-ion plasma engine, in which antiprotons annihilate with nucleons in a heavy atom nucleus to produce energetic charged nuclides and particles. The charged byproducts are confined by external magnetic field coils and collisionally transfer their energy to the remaining heavy atoms, forming a magnetically confined plasma. The magnetic mirror field is then relaxed at one end of the system, and the plasma escapes to provide thrust. By tailoring the antiproton and propellant injection rates, it may be possible to achieve a variety of thrust and specific impulse values using a single engine.

**Table 1 Proton-antiproton annihilation scheme**

| | | |
|---|---|---|
| $p + \bar{p} \rightarrow n\pi^+ + n\pi^- + m\pi^0$ | $n = 1.5, m = 2$ | $E(p\bar{p}) = 1877$ MeV |
| $\pi^0 \xrightarrow{2.2 \times 10^{-16}\ s} 2\gamma$ | $E_\gamma \simeq 130$–$300$ MeV | $KE(\pi^0) \simeq 220$ MeV |
| $\pi^+ \xrightarrow{7.0 \times 10^{-8}\ s} \mu^+ + \nu_\mu$ | $KE(\pi^+) \simeq 250$ MeV | $KE(\mu^+) \simeq 192$ MeV |
| $\pi^- \xrightarrow{7.0 \times 10^{-8}\ s} \mu^- + \bar{\nu}_\mu$ | $KE(\pi^-) \simeq 250$ MeV | $KE(\mu^-) \simeq 192$ MeV |
| $\mu^+ \xrightarrow{6.2 \times 10^{-6}\ s} e^+ + \nu_e + \bar{\nu}_\mu$ | $KE(\mu^+) \simeq 192$ MeV | $KE(e^+) \simeq 100$ MeV |
| $\mu^- \xrightarrow{6.2 \times 10^{-6}\ s} e^- + \nu_\mu + \bar{\nu}_e$ | $KE(\mu^-) \simeq 192$ MeV | $KE(e^-) \simeq 100$ MeV |
| $e^- + e^+ \rightarrow 2\gamma$ | $KE(e^\pm) \simeq 100$ MeV | $E_\gamma = 0.511$ MeV |

The efficiency of the pulsed heavy-ion plasma engine is limited by the amount of energy residing in the kinetic energy of the charged annihilation byproducts, estimated to be less than 20% of the initial annihilation energy[8]; of this amount, some fraction less than unity will be transferred to the plasma. Engine life may be limited by radioactive byproduct decay, neutron radiation damage, and neutral fragment sputtering of surrounding material. If instead the charged byproducts produced by antiproton annihilation in hydrogen were used, a variable thrust, variable specific impulse engine might be designed without the disadvantages of heavy atom annihilation. A computer model was thus constructed to predict the performance of an antiproton powered, magnetically confined hydrogen plasma engine.

## Antiproton Powered Plasma Engine

The system to be modeled is dynamic and complex. On one time scale, antiprotons annihilate with an initially neutral hydrogen gas to produce relativistic, charged pions. The pions traverse the hydrogen propellant and transfer some amount of energy before decaying into charged, relativistic muons over a time scale of several nanoseconds. The energetic muons interact with the hydrogen over microsecond time scales before decaying into extremely relativistic electrons and positrons. The electrons and positrons in turn give up energy to the hydrogen over a time scale corresponding to the plasma confinement time, typically a few milliseconds. The electrons and positrons are stable, although positrons may be lost due to annihilation with plasma electrons. Strong magnetic fields are used for confinement and stability, but even so particles will be continually lost from the system. Thus, at any given time the ensemble will consist of protons, antiprotons, plasma electrons, hydrogen atoms, pions($\pm$), muons($\pm$), decay electrons, and positrons, evolving and interacting on time scales which may vary over six orders of magnitude.

To simplify the system modeling, the $\pi^+$ and $\pi^-$ mesons are not distinguished, and are assumed to have an initial kinetic energy equal to the average distribution kinetic energy of 250 MeV/pion. Similarly, no distinction is made between the charged muons, which are assumed to have an initial kinetic energy of 192 MeV/muon. Muon decay produces electrons and positrons, and it is assumed that half of the electron/positron number density consists of electrons, the other half of positrons, each with an initial kinetic energy of 100 MeV/$e^{\pm}$. This separation allows an estimate to be made of positron depletion due to annihilation with plasma electrons. The assumption of indistinguishable particles is valid since Coulomb interactions and energy exchange rates are proportional to even powers of the particle charge. The possibility of relativistic $\pi^+\pi^-$ or $\mu^+\mu^-$ annihilation occurring in low pion or muon number densities over their respective lifetimes is remote and not considered in the model. The use of average initial kinetic energies is somewhat crude, but a comparison of energy loss rates calculated over the range of experimentally observed particle kinetic energies indicates the error introduced by this approximation is negligible.[9]

Rate equations are used to evaluate the antiproton and charged annihilation byproduct number densities at each time step. The time rate of change of the antiproton number density due to annihilation with the hydrogen propellant is

$$\frac{dn_{\bar{p}}}{dt} = -\lambda_\alpha(t) n_{\bar{p}} \tag{5}$$

where $n_{\bar{p}}(0)$ is the initial antiproton number density and $\lambda_\alpha$ is a time-dependent annihilation rate coefficient, given by

$$\lambda_\alpha(t) = (1 - \alpha) n_p \langle \sigma v \rangle_{\bar{p}H} + \alpha n_p \langle \sigma v \rangle_{p\bar{p}} \tag{6}$$

The quantity $n_p$ denotes the hydrogen propellant number density and $\alpha$ is the associated ionization fraction, which is calculated at each time step using a general Saha ionization equation. Assuming the antiprotons and hydrogen atoms (and/or protons) are in thermal equilibrium, a Maxwellian velocity distribution may be used to estimate the annihilation rate probabilities

$$\langle \sigma v \rangle = \frac{\int \langle \sigma v \rangle dn}{\int dn} \tag{7}$$

where

$$dn = n \left( \frac{\mu}{2\pi\kappa T} \right)^{3/2} v^2 \exp^{-\mu v^2/2\kappa T} dv \tag{8}$$

and $\mu$ is the proton-antiproton reduced mass. Substituting for $dn$ yields

$$\langle \sigma v \rangle = \frac{2.21 \times 10^4}{T^{1/2}(\text{eV})} \int_0^\infty \sigma(E_r) \frac{E_r}{T} \exp\left[ \frac{-E_r}{T} \right] dE_r m^3/s \tag{9}$$

where $\sigma$ is the appropriate annihilation cross section, $E_r$ is the relative interaction energy between annihilating particles, and $T$ is the hydrogen gas/plasma temperature. The cross sections for $\bar{p}H$ rearrangement collision annihilation and $p\bar{p}$ direct annihilation are given by Morgan and Hughes[6]; substituting for these cross sections and evaluating the annihilation reaction rate probabilities over the energies of interest yields

$$\begin{aligned} \langle \sigma v \rangle_{\bar{p}H} &\simeq 2.15 \times 10^{-15} \frac{m^3}{s} \quad (T \leq 10 \text{ eV}) \\ &\simeq 0 \qquad\qquad\quad (T > 10 \text{ eV}) \end{aligned} \tag{10}$$

for rearrangement annihilation and

$$\langle \sigma v \rangle_{p\bar{p}} \simeq \frac{1.13 \times 10^{-18}}{T^{1/2}(\text{eV})} \frac{m^3}{s} \quad (1 \text{ eV} \leq T \leq 10^4 \text{ eV}) \tag{11}$$

for direct annihilation. The rearrangement annihilation rate probability dominates at the beginning of the annihilation period when the hydrogen propellant is predominantly a cold, neutral gas. The direct annihilation rate probability becomes important as the hydrogen is heated and ionized by the annihilation byproducts, and dominates when the gas becomes fully ionized.

The production and decay of charged pions arising from the $\bar{p}H$ or $p\bar{p}$ annihilations is given by

$$\frac{dn_\pi}{dt} = 3\lambda_\alpha(t) n_{\bar{p}}(t) - \lambda_\pi n_\pi \tag{12}$$

where $\lambda_\pi$ is assumed to be the average pion decay constant, equal to $(70 \text{ ns})^{-1}$, and the factor of three takes into account the production of three charged pions per annihilation event. The decay of each charged pion produces one charged muon, which in turn decays in an average time of 6.2 $\mu$s into either an electron (from $\mu^-$ decay) or a positron (from $\mu^+$ decay). Since the $\mu^-$ and $\mu^+$ are treated as identical particles in this model, the rate equation for muons becomes

$$\frac{dn_\mu}{dt} = \lambda_\pi n_\pi - \lambda_\mu n_\mu \tag{13}$$

where $\lambda_\mu$ is taken to be the average muon decay constant, equal to $(6.2\ \mu\text{s})^{-1}$. The rate equation for electron/positron production can then be written

$$\frac{dn_{e^\pm}}{dt} = \lambda_\mu n_\mu \tag{14}$$

The electrons and positrons are stable particles and do not decay; however, the positrons may undergo annihilation with ambient plasma electrons. An electron-positron annihilation frequency may be calculated using

$$\nu_\alpha = n_e \sigma_e^{\pm} v_e^{\pm} \tag{15}$$

where $n_e$ is the plasma electron number density, $\sigma_e^{\pm}$ is the electron-positron annihilation cross section given by Morgan and Hughes,[6] and $v_e^{\pm}$ is the relative velocity between the positrons and plasma electrons. Thus, at each time step the number of positron annihilations can be calculated, and the electron/positron number density adjusted accordingly.

Relativistic forms of the energy loss equations derived by Bethe-Bloch[10] and Sivukhin[11] are used to estimate the energy transferred by the relativistic particles to the hydrogen propellant. For heavy particles in atomic hydrogen, the energy loss equation can be cast in the form[9]

$$\frac{dE}{dt} = -\frac{1.53 \times 10^{-14} n_e}{\beta}\left[\ell n\left(\frac{1.56 \times 10^{21} \beta^2}{\omega_{pe}\sqrt{1-\beta^2}}\right) + \frac{1}{2} - \beta^2\right]\frac{\text{eV}}{\text{sec}} \tag{16}$$

where $n_e$ is the plasma electron number density, $\omega_{pe}$ is the electron plasma frequency, and $\beta$ is the ratio v/c. For the energy loss of electrons and positrons in atomic hydrogen, the energy loss equation becomes[9]

$$\frac{dE}{dt} = -1.53 \times 10^{-14}\frac{n_e}{\beta}\left[\ell n\left(\frac{7.67 \times 10^{17}}{\omega_{pe}} T_{e^{\pm}}^{1/2}\right) - \frac{\ell n 2}{2}[2(1-\beta^2)^{1/2} - 1 + \beta^2] + 1 - \frac{\beta^2}{2} + \frac{1}{16}([1-(1-\beta^2)^{1/2}]^2)\right]\frac{\text{eV}}{\text{sec}} \tag{17}$$

where $T_{e^{\pm}}$ is the kinetic energy of the electron/positron created by muon decay, and the other symbols are defined as before.

The energy lost by a charged particle undergoing Coulomb collisions in a fully ionized plasma has been extensively reviewed by Sivukhin.[11] For an ionized plasma, the energy loss formula takes the much simpler form

$$\left\langle\frac{dE}{dt}\right\rangle = -\frac{4\pi e^2}{v}\Sigma^* \ell n \Lambda\, n^* e^{*2} \cdot\left[\frac{\Phi(\rho^* v)}{m^*} - \frac{2\rho^* v(m+m^*)}{m m^* \sqrt{\pi}} e^{-\rho^{*2} v^2}\right]\frac{\text{ergs}}{\text{sec}} \tag{18}$$

where the * denotes the Maxwellian field particles, $\Phi(x)$ is the error integral, defined by

$$\Phi(x) = \frac{2}{\sqrt{\pi}}\int_0^x e^{-\xi^2}\, d\xi \tag{19}$$

and the parameter $\rho^*$ is defined by

$$\rho^* \equiv \sqrt{\frac{m^*}{2T^*}} \tag{20}$$

where $T^*$ is the energy for a given field particle. The term $\ell n\, \Lambda$ is the Coulomb logarithm, which is given for relativistic energies by the quantum mechanical formula

$$\ell n\, \Lambda_{qu} = \ell n\, \Lambda_{cl} + \ell n \frac{2\alpha c}{v} - \frac{1}{2} \tag{21}$$

where $\ell n\, \Lambda_{cl}$ is the classical value of the Coulomb logarithm. For large values of $(\rho^* v)$, the energy loss can be approximated as

$$\left\langle\frac{dE}{dt}\right\rangle = -\frac{1.5 \times 10^{-14}}{\beta}\Sigma\frac{n^*\, \ell n \Lambda}{(m^*/m_e)}\frac{\text{eV}}{s} \tag{22}$$

where $m^*/m_e$ is the ratio of the field particle mass to the electron rest mass. The above equation may be used to estimate the energy lost by an incident particle to the plasma electrons versus the energy lost to the plasma ions

$$\left\langle\frac{dE}{dt}\right\rangle_e : \left\langle\frac{dE}{dt}\right\rangle_i = \left|\frac{m_i^* e}{m_e e_i^*}\right| \tag{23}$$

The particle gives up much more energy to the plasma electrons, and to heat the ion component requires that the heated plasma electrons impart energy to the ions. The energy exchange rate between the electrons and ions is given by

$$Q_{ei} = \frac{(T_e - T_i)}{\tau_{eq}^{ei}} \tag{24}$$

where $T_e(T_i)$ is the electron (ion) temperature and $\tau_{eq}^{ei}$ is the electron-ion energy equilibration time

$$\tau_{eq}^{ei} = 3.17 \times 10^{14}\frac{T_e^{3/2}(\text{eV})}{n_e(m^{-3})\, \ell n\, \Lambda}\, s \tag{25}$$

Bremsstrahlung and synchrotron radiation may be neglected for the energetic pions and muons,[9] but are important energy loss mechanisms for the relativistic electrons and positrons and are included in the simulation. Plasma synchrotron radiation is neglected, but plasma bremsstrahlung radiation, a dominant energy loss mechanism at higher temperatures and plasma number densities, is evaluated at each time step and the plasma energy adjusted accordingly. Deexcitation and recombination energy losses, which may appear as the plasma is heated from an initially neutral to fully ionized state, are small and are not included in the model. Additional details of the code structure may be found in Ref. 9.

#### Confinement and Stability

Magnetic fields are used to constrain the charged annihilation byproducts and confine the hydrogen plasma away from any material walls. The magnetic mirror system (Fig. 1) is assumed to consist of solenoidal current coils producing a longitudinal magnetic field and mirror field coils at each end of the system to provide particle containment and overall MHD stability.[12] Antiprotons are injected axially along magnetic field lines and the neutral hydrogen propellant is injected radially across the field lines. Once the plasma is heated, one end of the magnetic mirror system is relaxed, forming a magnetic nozzle and allowing the plasma to escape.

The minimum magnetic field strengths required to contain the system of relativistic particles and plasma propellant are

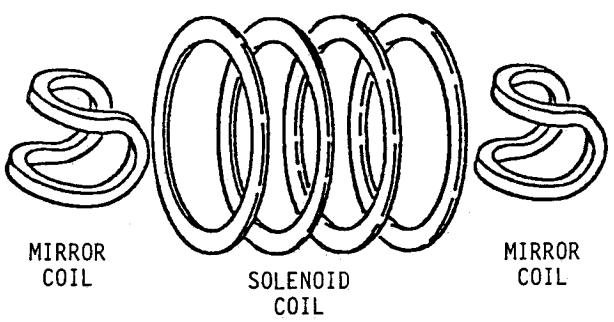


**Fig. 1 Magnetic mirror system.**

calculated by balancing the magnetic field pressure and the plasma/particle kinetic pressure

$$\frac{B^2}{2\mu_0} = \sum_j (nkT)_j \tag{26}$$

where $n$ is the number density and $kT$ is the energy of the $j^{th}$ species, and the summation extends over all particle species present in the system. An additional constraint on minimum field strengths is imposed by requiring the relativistic particle gyroradii to be much smaller than the reaction chamber dimensions, yielding a minimum magnetic field strength of about 10 Tesla for typical reaction chamber dimensions.[9]

The probability that a charged particle will be lost from the magnetic mirror system is given by[13]

$$P = 1 - \left(\frac{R_m - 1}{R_m}\right)^{1/2} \tag{27}$$

where $P$ is the probability of escape and $R_m$ is the magnetic mirror ratio, the ratio of the maximum to minimum magnetic field strengths. For a uniform magnetic field, the mirror ratio is unity and no particles are confined. As $R_m \to \infty$, the probability of escape goes to zero. Current technology restricts maximum magnetic field strengths in the mirror regions to well below 50 Tesla,[14] hence, the mirror ratio of the system will be limited to fairly low values. Loss probabilities are used in the simulation to modify the relativistic particle number densities at each time step. Plasma diffusion and end losses are assumed to be negligible over the millisecond plasma confinement times,[9] although in a real system plasma losses may increase by ambipolar diffusion through the mirrors or by a multitude of plasma microinstabilities leading to enhanced particle loss rates.[15] The assumption of a constant plasma number density during the heating and exhaust cycle thus provides a somewhat optimistic upper bound on the calculated engine performance.

#### Engine Performance

Energy transfer efficiencies for the engine are calculated using

$$\eta_i = \frac{E_i n_p}{(1877\ \text{MeV}) n_{\bar{p}}} \tag{28}$$

where $E_i$ is the gain in plasma ion energy, $n_p$ is the hydrogen propellant number density, $n_{\bar{p}}$ is the initial antiproton number density, and 1877 MeV is the amount of energy released in each proton-antiproton annihilation. Electron energies are omitted from the definition of engine efficiency, since only the plasma ions contribute substantially to the engine thrust.

Number densities are used in the simulation to provide flexibility in the choice of total reaction chamber volume. Once the chamber volume $V_c$ is selected, the hydrogen propellant mass flow rate may be calculated from

$$\dot{m}_p = \frac{m_p n_p V_c}{\Delta t} \tag{29}$$

where $m_p$ is the atomic mass of hydrogen, $n_p$ is the hydrogen propellant number density, and $\Delta t$ is the pulse repetition period of the engine. Similarly, the antiproton mass flow rate may be found using

$$\dot{m}_{\bar{p}} = \frac{m_{\bar{p}} n_{\bar{p}} V_c}{\Delta t} \tag{30}$$

where $m_{\bar{p}}$ and $n_{\bar{p}}$ are the antiproton rest mass and initial number density, respectively.

Engine thrust and specific impulse are estimated using the ideal rocket approximations.[16] An additional assumption is made that all of the ionized exhaust leaves the chamber axially with the same average energy directed by a 100% efficient magnetic nozzle. The exhaust velocity is then given by[9]

$$v_{ex} = 1.4 \times 10^4 \sqrt{E_i(\text{eV})}\, m/s \tag{31}$$

and the specific impulse ($I_{sp}$) of the engine is

$$I_{sp} = \frac{v_{ex}}{9.8\ m/s^2} \tag{32}$$

The thrust produced during each pulse is given by

$$Th = \dot{m}_p v_{ex} \tag{33}$$

and in terms of propellant number density may be written

$$Th = \frac{m_p n_p V_c}{\Delta t} v_{ex} \tag{34}$$

## Results and Discussion

The model was tested against an antiproton powered orbital-transfer vehicle (OTV) study performed by Cassenti.[9,17] The predictions of engine thrust and specific impulse agree with Cassenti's Monte Carlo simulations to within 5%. In addition, Monte Carlo simulations performed at the Jet Propulsion Laboratory (JPL) of the annihilation energy transfer efficiencies in a hydrogen plasma are in good agreement with the energy transfer efficiencies predicted by the code.[18]

Selected results are presented in the following sections for low, moderate, and high hydrogen propellant number densities and a range of antiproton number densities. Cases presented in the first part of each section assume no charged particles are lost from the system, and represent an upper limit on engine performance. Combinations leading to optimum propellant heating in each case are reexamined using finite magnetic mirror ratios to evaluate the effect of particle losses on engine performance. Mirror ratios of 2 and 3 are used in compliance with current technology constraints.[14] Antiproton and hydrogen injection energies are set at 0.1 eV to allow rapid injection into the reaction chamber, yet retain a sufficiently low center-of-mass velocity for efficient annihilation. Maximum electron and ion energies, annihilation energy transfer efficiencies, minimum magnetic field strength requirements, predicted specific impulse, and predicted thrust (normalized to reaction chamber volume and pulse repetition rate) are tabulated in each section, and examples of engine performance are given.

#### Low Number Density Hydrogen Plasma

The lowest hydrogen propellant number density considered in this study is $10^{20}$ m$^{-3}$. Figures 2a through 2d display antiproton, pion, muon, and relativistic electron/positron number density evolutions for initial antiproton number densities between $10^{15}$ m$^{-3}$ and $10^{18}$ m$^{-3}$, with no mirror losses. Antiproton annihilation becomes less efficient as the initial antiproton number density is increased, due to the rapid heating of the hydrogen propellant and the resulting decrease in proton-antiproton annihilation cross sections. The fraction of antiprotons remaining in the system after 1 ms increases from essentially zero at lower antiproton number densities to almost 70% for initial antiproton number densities of $10^{18}$ m$^{-3}$. The prolonged annihilation times reduce the peak byproduct number densities and spread their production over the confinement period.

Plasma ion energies are plotted for each of the initial antiproton number densities in Fig. 3. Comparing the number density evolutions with the temperature curves, it is clear that the electrons and positrons are primarily responsible for heating the plasma, with little or no contribution from the pions and muons. The continued production of particles during the

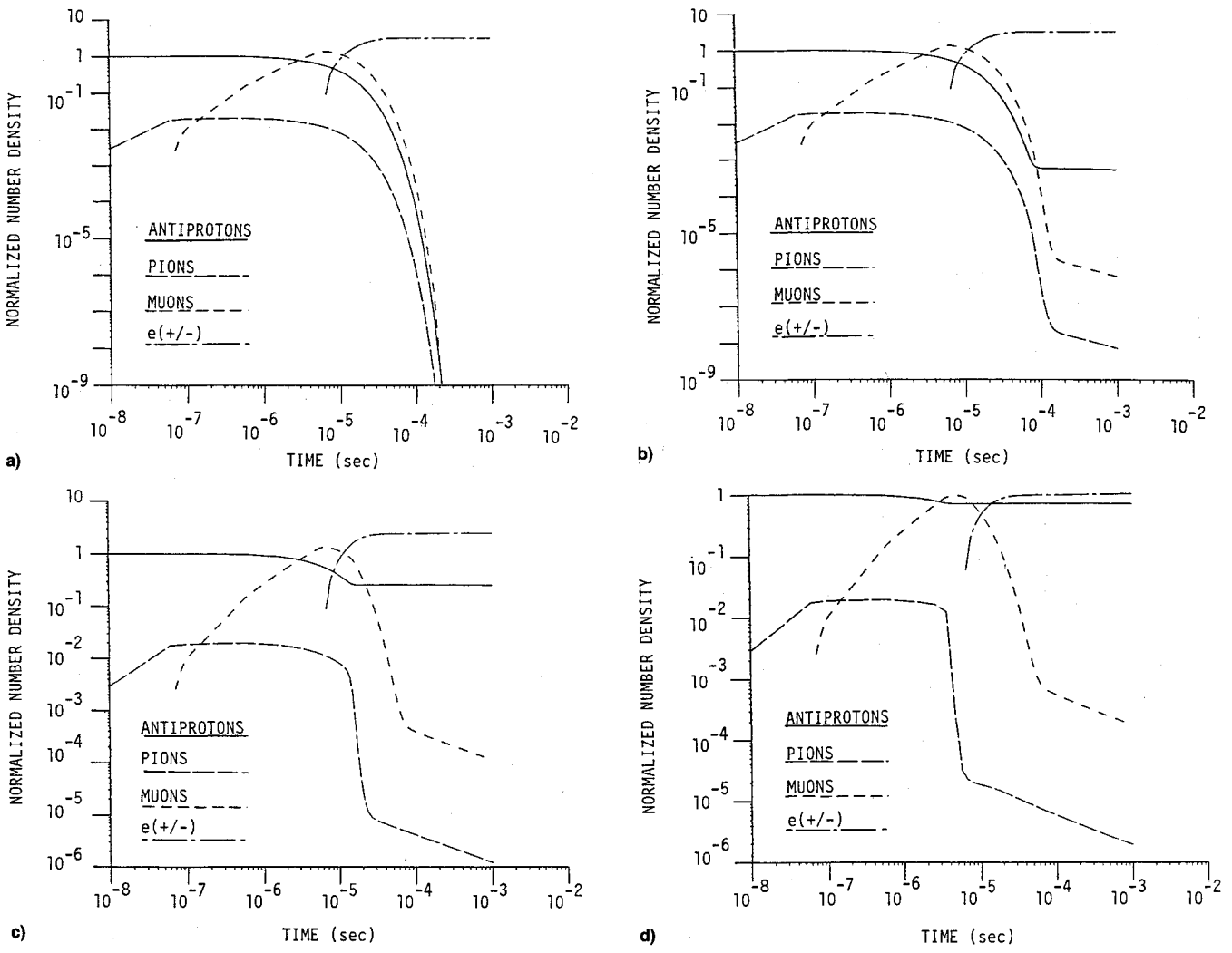


**Fig. 2** $\bar{P}$, $\pi$, $\mu$, and $e^{\pm}$ number density evolutions for $n_p = 10^{20}$ m$^{-3}$. a) $n_{\bar{p}} = 10^{15}$ m$^{-3}$. b) $n_{\bar{p}} = 10^{16}$ m$^{-3}$. c) $n_{\bar{p}} = 10^{17}$ m$^{-3}$. d) $n_{\bar{p}} = 10^{18}$ m$^{-3}$. No mirror losses.

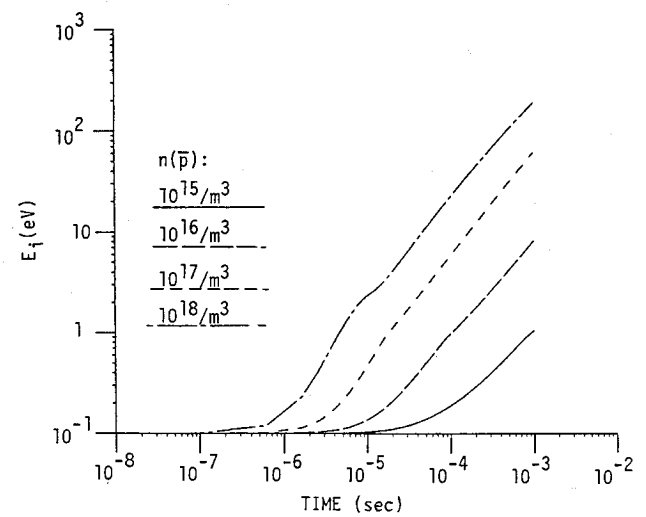


**Fig. 3 Plasma ion energy versus time for various initial antiproton number densities.** $n_p = 10^{20}$ m$^{-3}$. **No mirror losses.**

prolonged annihilation times slowed program execution considerably, and computer runs were terminated at 1-ms confinement times for economy. Test runs performed out to 5 ms indicate that plasma temperatures increase linearly with increasing confinement time.

Table 2 summarizes the results for the low number density hydrogen plasma engine. Maximum propellant temperatures are achieved at higher antiproton number densities, but at the expense of wasting antiproton fuel. In addition, the tabulated energies indicate that the plasma electrons are being heated faster than they can share their energy with the ions, and the plasma moves away from thermal equilibrium as the initial antiproton number density is increased. At lower mirror ratios, the loss of pions from the system results in a lower muon production rate, and the combined loss of pions and muons results in decreased electron/positron production. The reduced electron/positron production rate, coupled with their continual loss from the magnetic mirror system, significantly diminishes the propellant temperature and associated engine performance.

The above results suggest that the optimum antiproton number density is around $10^{16}$ m$^{-3}$ for the low density hydrogen propellant engine. With a mirror ratio of 3, the maximum ion energy is about 4.5 eV after 1-ms, yielding a low annihilation energy transfer efficiency of 0.0024%. Assuming a 5 ms confinement time, the ion temperature climbs to roughly 22.5 eV and the efficiency increases to approximately 0.012%. The calculated magnetic field strengths required for confinement are smaller than the 10 Tesla field required to constrain the pion gyroradii to reasonable values ($\leq$0.1 m), and are primarily due to relativistic particle kinetic pressure rather than plasma thermal pressure.

For the optimum case outlined above, a 1-ms plasma confinement time yields a specific impulse of 3030 seconds and a normalized thrust of $5.0 \times 10^{-4}$ N · s/m$^3$, where the thrust has been normalized to the reaction chamber volume and engine pulse period. Assuming the reaction chamber has a radius of 1 meter and a length of 10 meters, and assuming a

**Table 2 Engine performance parameters for hydrogen propellant number density of $10^{20}$ m$^{-3}$[a]**

| $n_p$(m$^{-3}$) | $R_m$ | $E^e_{max}$ (eV) | $E^i_{max}$ (eV) | $\eta_i$ | $B_{min}(T)$ | $I_{sp}(s)$ | $Th$(N · sec/m$^3$) |
|---|---|---|---|---|---|---|---|
| $10^{15}$ | ∞ | 1.0 | 1.0 | $5.3 \times 10^{-5}$ | 0.35 | 1430 | $2.3 \times 10^{-4}$ |
| $10^{16}$ | ∞ | 8.1 | 8.1 | $4.3 \times 10^{-5}$ | 1.1 | 4040 | $6.6 \times 10^{-4}$ |
| $10^{16}$ | 3 | 4.5 | 4.5 | $2.4 \times 10^{-5}$ | 0.81 | 3030 | $5.0 \times 10^{-4}$ |
| $10^{16}$ | 2 | 3.0 | 3.0 | $1.6 \times 10^{-5}$ | 0.65 | 2475 | $4.1 \times 10^{-4}$ |
| $10^{17}$ | ∞ | 66 | 60 | $3.2 \times 10^{-5}$ | 3.1 | 11100 | $1.8 \times 10^{-3}$ |
| $10^{18}$ | ∞ | 370 | 190 | $1.0 \times 10^{-5}$ | 8.5 | 19700 | $3.3 \times 10^{-3}$ |

[a]Confinement time = 1 ms; energy and efficiency parameters increase linearly with time for longer confinement times. Thrust is normalized to chamber volume and engine pulse period.

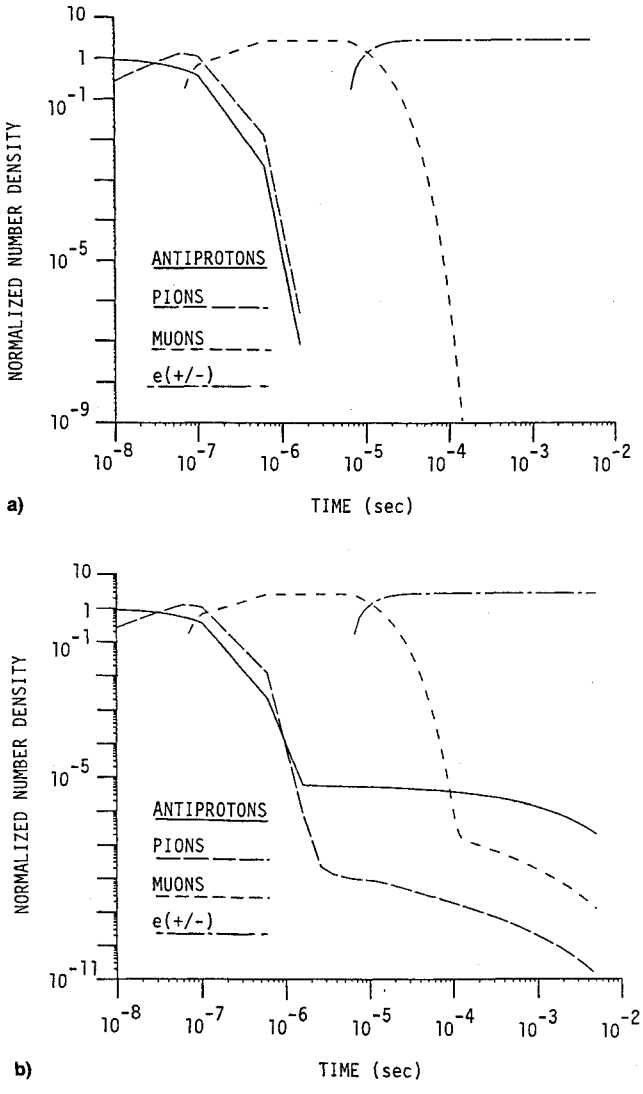


**Fig. 4 $\bar{P}$, $\pi$, $\mu$, and $e^{\pm}$ number density evolutions for $n_p = 10^{22}$ m$^{-3}$. a) $n_{\bar{p}} = 10^{15}$ m$^{-3}$. b) $n_{\bar{p}} = 10^{18}$ m$^{-3}$. No mirror losses.**

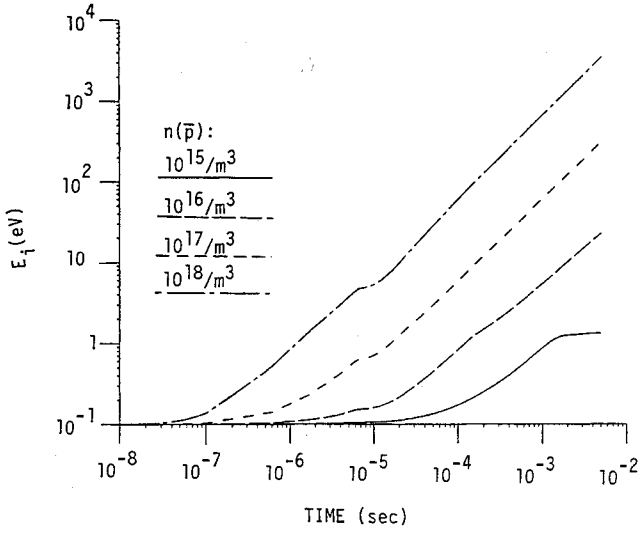


**Fig. 5 Plasma ion energy versus time for various initial antiproton number densities. $n_p = 10^{22}$ m$^{-3}$. No mirror losses.**

pulse period of 10 ms, the equivalent continuous thrust is only 16 N (3.5 lbf). Increasing the plasma confinement time to 5 ms raises the specific impulse to 5530 s with an associated equivalent continuous thrust of 30 N (6.6 lbf). In both cases the hydrogen propellant flow rate is $3.1 \times 10^{21}$ H/pulse (525 mg/s) and the antiproton flow rate is $3.1 \times 10^{17}$ $\bar{p}$/pulse (52.5 $\mu$g/s), since thrust is normalized to the engine pulse period and not the plasma confinement time.

The low energy transfer efficiencies associated with the low hydrogen propellant number density severely limit the potential performance of the plasma engine. Increasing the hydrogen number density results in higher energy transfer efficiencies and improves engine performance, as shown in the following section.

### Moderate Number Density Hydrogen Plasma

A hydrogen propellant number density of $10^{22}$ m$^{-3}$ was chosen to model the performance of a moderate number density hydrogen plasma engine. Figures 4a and 4b show the antiproton and annihilation byproduct number density evolutions for initial antiproton number densities of $10^{15}$ m$^{-3}$ and $10^{18}$ m$^{-3}$, respectively, with no mirror losses. Number density evolutions for intermediate antiproton number densities are similar to those shown in Fig. 4a. At the lower antiproton number densities, essentially complete antiproton annihilation takes place during the 5 ms confinement time. Pion number densities reach a maximum slightly in excess of the initial antiproton number densities before decaying from the system. Muon number densities climb to nearly 3 times the initial antiproton number densities before decaying, in agreement with the initial assumption of three charged mesons produced per annihilation event. The electron/positron number densities reach 3 times the initial antiproton number density as the muons decay, and remain constant at this level. Increasing the initial antiproton number density to $10^{18}$ m$^{-3}$ heats the hydrogen too rapidly, decreasing the annihilation cross sections and prolonging the period of proton-antiproton annihilation. At the end of 5 ms, nearly $10^{12}$ m$^{-3}$ antiprotons remain in the system, and will be exhausted with the plasma propellant.

Figure 5 shows the ion energy evolution for each of the initial antiproton number densities. The flattening of the energy curve for the case $n_{\bar{p}} = 10^{15}$ m$^{-3}$ is due to plasma bremsstrahlung radiation; the energy deposited in the plasma by the charged annihilation products is balanced by radiation losses, with no net gain in plasma energy. Energy deposition rates associated with the higher initial antiproton number densities exceed the rate at which bremsstrahlung radiation is lost, resulting in steadily increasing propellant temperatures. Also evident is the increased plasma energies caused by the

relativistic muons and, to a lesser extent, the relativistic pions. At higher initial antiproton number densities the muons may substantially heat the plasma before decaying from the system.

Minimum magnetic field profiles for each of the above cases are presented in Fig. 6. In each case, the minimum calculated field strength is due primarily to the relativistic particle kinetic pressure, which greatly exceeds the plasma thermal pressure. The evolution of the minimum magnetic field strength closely follows the production and decay of the charged annihilation byproducts (Fig. 4). For initial antiproton number densities of $10^{18}$ m$^{-3}$, the minimum field strength required for particle confinement is approximately 14 Tesla. The use of finite mirror ratios reduced both the minimum magnetic field strengths required for confinement and the final plasma ion temperatures, due to the loss of relativistic charged particles from the magnetic mirror system.

Table 3 lists plasma and engine performance parameters for the moderate number density plasma engine. Energy transfer efficiencies are greatly improved over the low number density cases presented previously, and complete antiproton annihilation occurs under most operating conditions. A respectable range of thrust and specific impulse values are available for reasonable antiproton mass injection rates and magnetic mirror ratios, which may allow some flexibility in mission designs.

Assuming a reaction chamber radius of 1 meter, length of 10 meters, and engine pulse period of 10 ms yields a hydrogen propellant mass flow rate of $3.14 \times 10^{23}$ H/pulse (52.5 g/s). For an antiproton number density of $10^{16}$ m$^{-3}$, the antiproton mass flow rate is $3.14 \times 10^{17}$ $\bar{p}$/pulse (52.5 $\mu$g/s). Using a mirror ratio of 3 yields a maximum ion energy of 10.4 $eV$ over a 5 ms plasma confinement time. The predicted specific impulse is 4610 s, and the normalized thrust is 0.76 N · s/m$^3$, which for the above parameters yields an equivalent continuous thrust of 2,400 N (535 lbf) with an energy transfer efficiency of 0.55%. Increasing the initial antiproton number density to $10^{18}$ m$^{-3}$ requires an antiproton mass flow rate of $3.14 \times 10^{19}$ $\bar{p}$/pulse (52.5 mg/s), and results in a maximum ion energy of 1765 eV for an energy transfer efficiency of 0.94%. The specific impulse is raised to an excessive 60,000 s, and the normalized thrust is 9.8 N · s/m$^3$ for an equivalent continuous thrust of 30,400 N (6800 lbf). The specific impulse might be lowered and the thrust increased by mixing a cold propellant gas with the hot plasma propellant before exhausting.

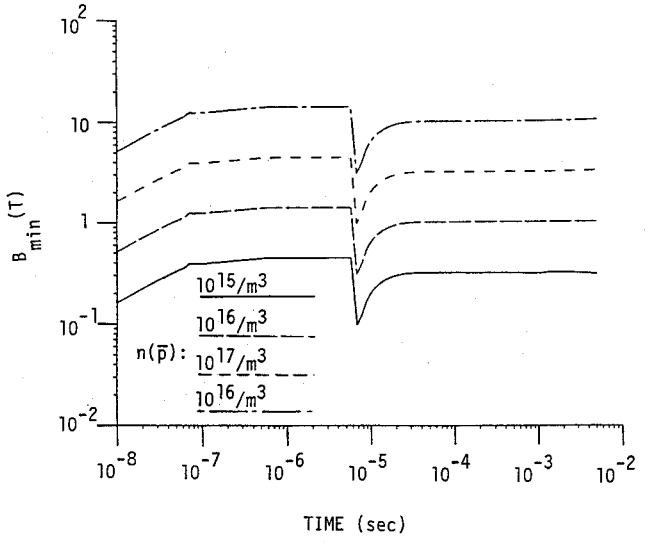


**Fig. 6 Minimum required magnetic field strength versus time for various initial antiproton number densities. $n_p = 10^{22}$ m$^{-3}$. No mirror losses.**

### High Number Density Hydrogen Plasma

Based on the previous results, it is expected that increasing the hydrogen number density will increase both the energy transferred to the plasma by the charged annihilation products

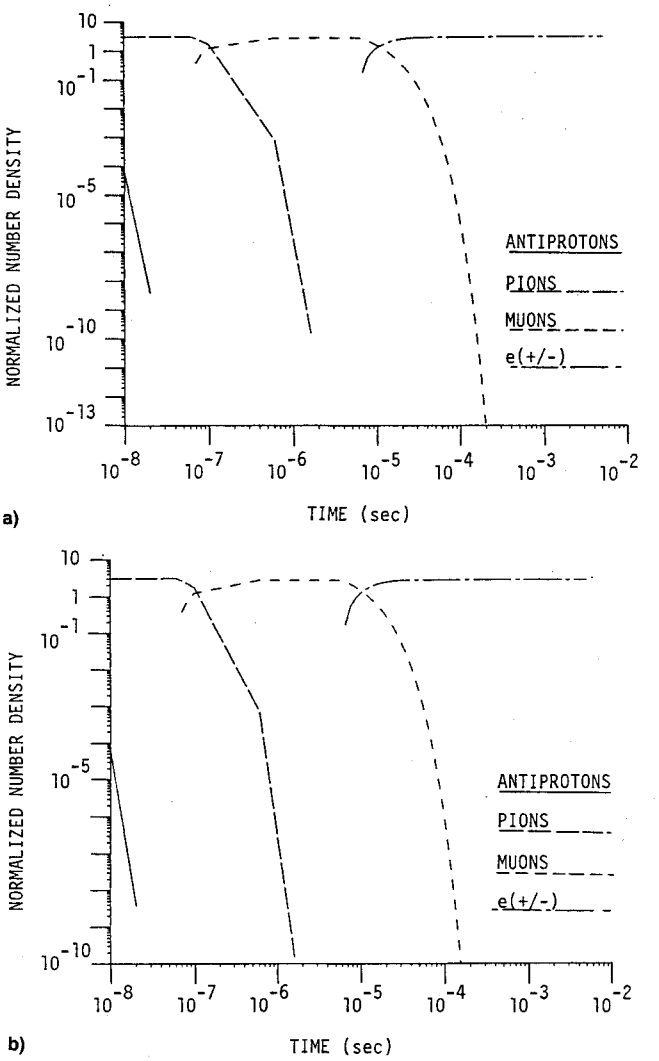


**Fig. 7 $\bar{P}$, $\pi$, $\mu$, and $e^{\pm}$ number density evolutions for $n_p = 10^{24}$ m$^{-3}$. a) $n_{\bar{p}} = 10^{16}$ m$^{-3}$. b) $n_{\bar{p}} = 10^{19}$ m$^{-3}$. No mirror losses.**

**Table 3 Engine performance parameters for hydrogen propellant number density of $10^{22}$ m$^{-3}$[a]**

| $n_{\bar{p}}$(m$^{-3}$) | $R_m$ | $E^e_{max}$ (eV) | $E^i_{max}$ (eV) | $\eta_i$ | $B_{min}(T)$ | $I_{sp}(s)$ | $Th$(N · sec/m$^3$) |
|---|---|---|---|---|---|---|---|
| $10^{15}$ | ∞ | 1.3 | 1.3 | $6.9 \times 10^{-3}$ | 0.32 | 1630 | 0.27 |
| $10^{16}$ | ∞ | 22 | 22 | $1.2 \times 10^{-2}$ | 1.4 | 6700 | 1.1 |
| $10^{16}$ | 3 | 10.4 | 10.4 | $5.5 \times 10^{-3}$ | 0.75 | 4610 | 0.76 |
| $10^{17}$ | ∞ | 295 | 294 | $1.6 \times 10^{-2}$ | 4.4 | 24500 | 4.0 |
| $10^{17}$ | 3 | 152 | 152 | $8.1 \times 10^{-3}$ | 2.4 | 17600 | 2.9 |
| $10^{18}$ | ∞ | 3470 | 3280 | $1.7 \times 10^{-2}$ | 14 | 81800 | 13 |
| $10^{18}$ | 3 | 1806 | 1765 | $9.4 \times 10^{-3}$ | 12 | 60000 | 9.8 |
| $10^{18}$ | 2 | 1140 | 1125 | $6.0 \times 10^{-3}$ | 10 | 48000 | 7.9 |

[a]Confinement time = 5 ms. Thrust is normalized to chamber volume and engine pulse period.

and the energy lost from the plasma by radiation. The highest hydrogen number density considered in the study is $10^{24}$ m$^{-3}$, and Figs. 7a and 7b display charged particle number density evolutions corresponding to initial antiproton number densities of $10^{16}$ m$^{-3}$ and $10^{19}$ m$^{-3}$, respectively. The nearly identical figures bracket the range of antiproton number densities used in the high propellant number density simulations. Complete antiproton annihilation occurs within 100 ns in all cases, and each of the pion, muon, and electron/positron number densities in turn reach maximum values 3 times higher than the initial antiproton number density. Due to the brief but intense antiproton annihilation period, the pions completely decay from the system within a few microseconds and the muons are depleted within fractions of a millisecond, which leaves the relativistic electrons and positrons to heat the plasma over the remaining confinement time.

The ion energy evolution (Fig. 8) displays several remarkable features. At low antiproton number densities, the ion energy is limited by plasma bremsstrahlung radiation to values slightly over 1 eV. Increasing the initial antiproton number density to $10^{17}$ m$^{-3}$ raises the ion energy only slightly to 1.8 eV, again due to plasma radiation losses offsetting charged particle energy deposition. Increasing the initial antiproton number density still further results in a substantial heating of the plasma as the energy deposited by the charged annihilation products exceeds the plasma energy lost by radiation. The role of the pions and muons in heating the plasma becomes more evident, although the net energy deposition from these particles is limited by plasma bremsstrahlung to fairly low values. The bulk of the plasma heating is again due to the relativistic electrons and positrons, which dominate the plasma radiation losses and raise the propellant temperature several orders of magnitude in a short period of time. Each of the energy curves are seen to peak at a time of 400 $\mu$s, after which the plasma energy falls rapidly to below 1 eV. A consideration of the energy loss equations shows that at this time the relativistic electrons and positrons have given up essentially all of their energy to the plasma, and with no source of heating the plasma rapidly loses energy by bremsstrahlung radiation. As the plasma cools it recombines, and confinement will be lost as the neutral hydrogen escapes through the magnetic fields. Consequently, to run the engine efficiently at high propellant number densities requires that the injection, heating, and exhaust cycle all be performed within 400 $\mu$s, or plasma cooling and neutral propellant loss will diminish the performance of the engine.

Figure 9 shows the minimum magnetic field strengths required to confine the system of charged decay particles and

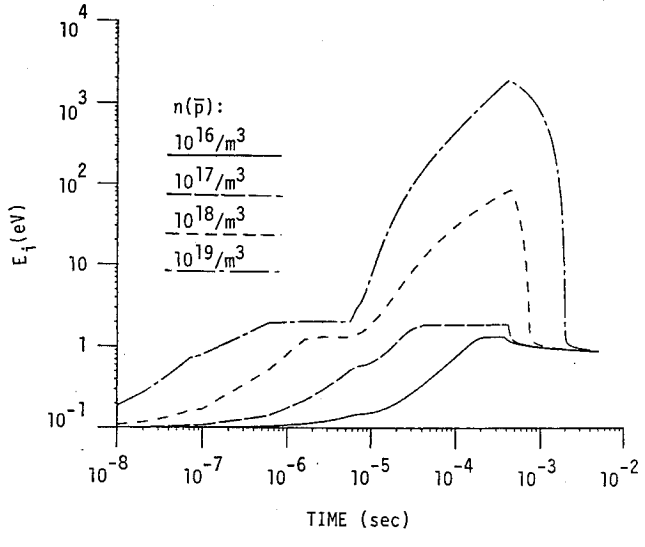


**Fig. 8 Plasma ion energy versus time for various initial antiproton number densities. $n_p = 10^{22}$ m$^{-3}$. No mirror losses.**

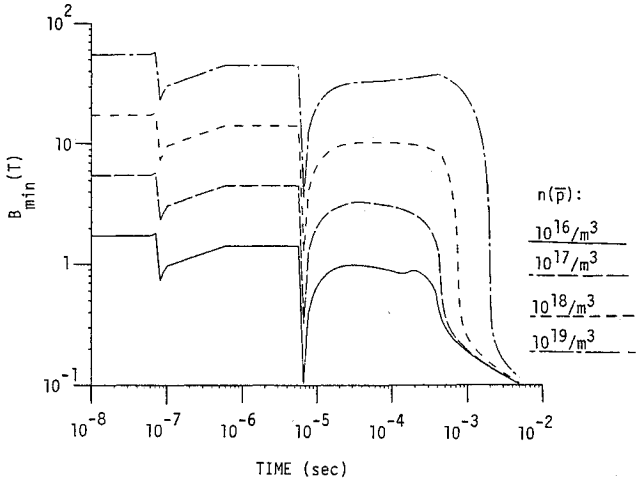


**Fig. 9 Minimum required magnetic field strength versus time for various initial antiproton number densities. $n_p = 10^{22}$ m$^{-3}$. No mirror losses.**

plasma. At low antiproton number densities, the field strengths are below the 10 Tesla field minimum set by particle orbit constraints. As the initial antiproton number density is increased to $10^{18}$ m$^{-3}$, the minimum field increases to 18 Tesla. The evolution of the magnetic field strengths follows the production and decay of the charged annihilation products and the heating and subsequent cooling of the hydrogen plasma. Increasing the initial antiproton number density to $10^{19}$ m$^{-3}$ requires a minimum confining field strength of nearly 60 Tesla for the central field, clearly beyond the capability of current or projected magnetic containment technology. Thus, the optimum antiproton number density at which to run the high propellant number density plasma engine is around $10^{18}$ m$^{-3}$; higher antiproton number densities require unrealistic magnetic field strengths to confine the system. Plasma heating due to lower antiproton number densities is significantly diminished by plasma bremsstrahlung radiation.

Performance parameters for the high number density hydrogen propellant engine are summarized in Table 4. The maximum ion energy reaches 81 eV for the optimum case outlined above with no particle losses. The ion energy is reduced to 28 eV for a mirror ratio of 3, and to 12 eV for a mirror ratio of 2. The corresponding magnetic field strengths are reduced from 18 Tesla with no mirror losses to 16 Tesla when $R_m = 3$ and 15 Tesla when $R_m = 2$, indicating that the relativistic charged particle pressure rather than the plasma thermal pressure plays the dominant role in defining the minimum magnetic field strengths. Using a mirror ratio of 2, the specific impulse is 4950 s, and the normalized engine thrust is 81 N · s/m$^3$. Assuming a 1 m by 10 m reaction chamber, a 10 ms engine repetition period, and the propellant is exhausted at its peak temperature within 400 $\mu$s, yields an equivalent continuous thrust of $2.5 \times 10^5$ N ($5.6 \times 10^4$ lbf) with an energy transfer efficiency of 0.64%.

## Shielding

Copious amounts of radiation are produced both by antiproton annihilations and by the confined plasma. Sensitive ship components must be protected, and the additional mass of a radiation shield will reduce the amount of payload the rocket can transport. Cassenti[19] has performed a preliminary numerical analysis of the crew shielding required for an antiproton powered OTV spacecraft. The crew is assumed to be located 100 meters away from the radiation source, and a tungsten shadow shield is placed between the crew and the annihilation chamber. The radiation source consists of the 200 MeV (average energy) gamma rays produced by prompt neutral pion decay. The simulation models pair creation, ionized energy loss, and positron annihilation production of secondary gamma rays within the shield material, but neglects the

**Table 4 Engine performance parameters for hydrogen propellant number density of $10^{22}$ $m^{-3}$[a]**

| $n_{\bar{p}}(m^{-3})$ | $R_m$ | $E^e_{max}$ (eV) | $E^i_{max}$ (eV) | $\eta_i$ | $B_{min}(T)$ | $I_{sp}(s)$ | $Th(N \cdot sec/m^3)$ |
|---|---|---|---|---|---|---|---|
| $10^{16}$ | $\infty$ | 1.3 | 1.3 | $6.9 \times 10^{-2}$ | 1.8 | 1630 | 27 |
| $10^{17}$ | $\infty$ | 1.8 | 1.8 | $9.6 \times 10^{-3}$ | 5.7 | 1920 | 31 |
| $10^{18}$ | $\infty$ | 81 | 81 | $4.3 \times 10^{-2}$ | 18 | 12860 | 210 |
| $10^{18}$ | 3 | 28 | 28 | $1.5 \times 10^{-2}$ | 15.7 | 7560 | 120 |
| $10^{18}$ | 2 | 12 | 12 | $6.4 \times 10^{-3}$ | 14.6 | 4950 | 81 |
| $10^{19}$ | $\infty$ | 1780 | 1780 | $9.5 \times 10^{-2}$ | 57 | 60300 | 990 |

[a]Confinement time = 400 $\mu$s. Thrust is normalized to chamber volume and engine pulse period.

production of high energy electrons created by ionization and Compton scattering of secondary particles. The high energy electrons will be a source of secondary gamma radiation due to bremsstrahlung emission. The simulation underestimates the number of lower energy gamma rays produced in the shielding material. The simulation is one dimensional, hence radiation scattering is also neglected. Assuming 8 mg of mass are annihilated, the model predicts a minimum shield thickness of 6.5 cm for adequate crew shielding. The estimated mass of the shield is thus on the order of $3.9 \times 10^3$ kg. The $10^4$ kg payload assumed in the OTV study must now include this mass, reducing the deliverable payload by nearly 40%.

Additional mass will be required to protect the superconducting coils, which are immediately outside the reaction chamber. Based on the above radiation model, and assuming the coils are placed 1 meter from the radiation source, an additional 11.8 cm of tungsten will be required to protect the OTV magnetic field coils.[9] Assuming a blanket shield is used around the entire reaction chamber, the required shield mass is $2.8 \times 10^4$ kg, or nearly 3 times larger than the $10^4$ kg payload assumed in the OTV mission study. Shadow shielding of the superconducting coils could reduce the required shielding mass, although protecting the coils from scattered radiation may limit any potential mass reduction.

The problem is exacerbated for the antiproton powered plasma engine operating at high temperatures, since plasma bremsstrahlung radiation must now be included in the total dosage calculations. Unlike the penetrating 200 MeV gammas, the lower energy bremsstrahlung photons will deposit most of their energy in the surface layers of the shield material, leading to shield ablation and degradation. A rough estimate of the maximum energy radiated by the engine is made by assuming an antiproton number density of $10^{18}$ $m^{-3}$, a hydrogen plasma number density of $10^{24}$ $m^{-3}$, and a plasma temperature of 10 eV (corresponding to the high propellant number density case with a mirror ratio of 2). Again, assuming a chamber radius of 1 m and a length of 10 m, this yields a chamber volume of 31 $m^3$. The total gamma radiation produced in each 400 $\mu$s pulse by neutral pion decay is approximately

$$E_\gamma \approx 10^{24} \cdot 31 \cdot 2 \cdot 2 \cdot 200 \text{ MeV} \approx 4.0 \text{ GJ} \qquad (35)$$

where it is assumed that 2 neutral pions are created in each annihilation event and each subsequently decays into two 200 MeV gamma rays. The plasma radiates an additional $6.6 \times 10^8$ $J$ each pulse, for a total radiated energy of 4.7 GJ/pulse. Dividing by the chamber surface area yields a total dosage of about 75 $MJ/m^2$ per pulse; an engine repetition rate of 10 ms would thus produce 7.5 $GW/m^2$. Assuming the superconducting coil cooling system can remove the equivalent of a few Watts/$m^2$ requires a shield thickness on the order of 17 cm, for a total shield mass of $2.24 \times 10^5$ kg. The equivalent continuous thrust produced by the engine is around $2.5 \times 10^5$ N over a 10 ms engine cycle. Assuming the shield mass dominates the total mass of the engine yields an average acceleration of about 1 $m/s^2$. To reach a velocity of 5.5 km/s (suitable for an OTV mission) requires an operating time of approximately 5500 s (1.5 h). The expended propellant mass is on the order of $2.9 \times 10^4$ kg and the required antiproton mass is 28.5 grams.

Since the radiation shield absorbs significant power, it must be cooled either actively or by passive radiative cooling. The additional mass of the cooling system will further reduce the available payload fraction, and design studies are required to determine the optimum method of dissipating the energy imparted to the shield. It may be possible to mitigate the mass penalty associated with the shielding and shield cooling system by tapping some of the energy deposited in the shield for use in an auxiliary power system.[19] The increase in shield temperature caused by absorbing an amount of energy $E$ is given by

$$\Delta T = \frac{E}{Jc_pM} \qquad (36)$$

where $c_p$ is the specific heat of the shield material (33 cal/kg°C for tungsten), $J$ is the mechanical equivalent of heat (4.186 $J$/cal), and $M$ is the shield mass. The temperature of a $2.3 \times 10^5$ kg tungsten shield absorbing roughly 5 GJ/pulse would increase about 160°C/pulse. Depending on the rate at which energy was removed from the shield, the steady state temperature could be much higher, providing a useful reservoir of energy for additional power requirements.

## Conclusion

Performance parameters for a pulsed, antiproton powered, magnetically confined hydrogen plasma engine were evaluated over several operating regimes. The engine suffers from extremely low energy transfer efficiencies at low hydrogen number densities and from excessive plasma bremsstrahlung at high hydrogen number densities. Optimum performance was obtained with a hydrogen number density of $10^{22}$ $m^{-3}$ and antiproton number densities between $10^{16}$ $m^{-3}$ and $10^{18}$ $m^{-3}$. Low to moderate thrust ($\leq$30 kN) over a wide range of specific impulse values (4600 s to 60,000 s) were generated using this moderate hydrogen number density for 5 ms plasma confinement times and realistic magnetic mirror systems. Energy transfer efficiencies were generally below 1%, with relativistic electrons and positrons providing most of the plasma heating. Higher thrust could be produced with higher hydrogen number densities, but the plasma will radiatively cool and recombine if it is not expelled within a few hundred microseconds after injection. Assuming the plasma can be fully exhausted from a realistic magnetic mirror system at its peak temperature, the high number density hydrogen propellant can produce a maximum specific impulse of 4950 s with an equivalent continuous thrust on the order of 250 kN.

Apart from the formidable problem of generating and storing sufficient antiproton fuel, the key engineering issues facing the magnetically confined pulsed plasma engine[9] are the design and construction of the superconducting magnetic field coils, efficient pulsed coil operation, antiproton transport into the annihilation region, and radiation shielding. Preliminary analysis indicates that substantial mass will be required to shield the superconducting coils from the high energy gamma radiation emitted in the $p\bar{p}$ annihilation process. Shielding problems are compounded by plasma bremsstrahlung radiation, which will contribute to shield surface ablation and degradation. The mass of the radiation shield may dominate the

total engine mass and significantly impact engine performance.

## Acknowledgments

This report is based on dissertation research performed at the University of New Mexico, Albuquerque, New Mexico. The author is indebted to Norman Roderick, Department of Chemical and Nuclear Engineering, UNM, for his counseling and guidance during the course of this project. Special thanks to Felix Huber, Universtität Stuttgart, West Germany, for comments and corrections to equations originally appearing in the UNM dissertation. Computer simulations were performed at the NASA Lewis Research Center, Cleveland, Ohio.

## References

[1]Massier, P. F., "The Need for Expanded Exploration of Matter-Antimatter Annihilation for Propulsion Applications," *Journal of the British Interplanetary Society*, Vol. 35, No. 9, 1982, pp. 387–390.

[2]Sanger, E., "Zur Theorie der Photoneraketen" ("The Theory of Photon Rockets"), *Ingenieur-Archiv*, Vol. 21, 1953, pp. 213–226.

[3]Nordley, Maj. G. U.S.A.F., 1989 personal communication.

[4]Forward, R. L., "Antiproton Annihilation Propulsion," AFRPL TR-85-034, AFRPL/LKC, Edwards AFB, CA, Sept. 1985.

[5]Morgan, D. L., "Concepts for the Design of an Antimatter Annihilation Rocket," *Journal of the British Interplanetary Society*, Vol. 35, No. 9, 1982, pp. 405–412.

[6]Morgan, D. L., and Hughes, V. M., "Atomic Processes Involved in Matter-Antimatter Annihilation," *Physical Review*, Vol. D-2, No. 8, 1979, pp. 1389–1391.

[7]Agnew, L. E., Jr., Elioff, T., Fowler, W. G., Lander, R. L., Powell, W. M., Segre, E., Steiner, H. M., White, H. S., Wiegand, C., and Ypsilantis, T., "Antiproton Interactions in Hydrogen and Carbon Below 200 MeV," *Physical Review*, Vol. 118, No. 5, 1960, pp. 1371–1391.

[8]Morgan, D. L., "Annihilations of Antiprotons in Heavy Nuclei," AFRPL TR-86-011, AFRPL/LKC, Edwards Air Force Base, CA, April 1986.

[9]LaPointe, M. R., "Antiproton Annihilation Propulsion with Magnetically Confined Plasma Engines," Ph.D. Dissertation, The University of New Mexico, Albuquerque, NM, May 1989.

[10]Sternheimer, R. M., "Fundamental Principles and Methods of Particle Detection," *Methods of Experimental Physics: Nuclear Physics*, Vol. 5-A, edited by L. C. L. Yuan and C. S. Wu, Academic Press, New York, 1961, pp. 1–288.

[11]Sivukhin, D. V., "Coulomb Collisions in a Fully Ionized Plasma," *Reviews of Plasma Physics*, Vol. 4, edited by M. A. Leontovich, Consultants Bureau, New York, 1966, pp. 93–240.

[12]Post, R. F., "Experimental Base of Mirror-Confinement Physics," *Fusion*, Academic Press, Vol. 1-A, edited by E. Teller, 1981, pp. 369–402.

[13]Glasstone, S., and Lovberg, R. H., *Controlled Thermonuclear Reactions*, D. van Nostrand Company, Inc., Princeton, NJ, 1960, pp. 366–400.

[14]Herlach, F. (ed), *Strong and Ultrastrong Magnetic Fields and Their Applications*, *Topics in Applied Physics*, Vol. 57, Springer-Verlag, Berlin, 1985, pp. 205–349.

[15]Miyamoto, K., *Plasma Physics for Nuclear Fusion*, MIT Press, Cambridge, MA, 1980, chapt. 8–16.

[16]Sutton, G. P., *Rocket Propulsion Elements*, 2nd ed., J. Wiley & Sons, New York, 1985, pp. 45–53.

[17]Cassenti, B. N., "Antimatter Propulsion for OTV Applications," *Journal of Propulsion and Power*, Vol. 1, No. 2, 1985, pp. 143–149.

[18]Callas, J., "The Application of Monte Carlo Modeling to Matter-Antimatter Annihilation Propulsion Concepts," JPL D-6830, Jet Propulsion Laboratory, California Institute of Technology, Pasadena, CA, October 1, 1989, pp. 10–12.

[19]Cassenti, B. N., "Radiation Shield Analysis for Antimatter Rockets," United Technologies Research Center, East Hartford, CT, 1987.